AGU PUBLICATIONS

JGR

Journal of Geophysical Research: Solid Earth

RESEARCH ARTICLE
10.1002/2014JB010983

Key Points:
- We test three different conceptual models of sub-slab mantle anisotropy
- A model where sub-slab splitting varies with age best matches the observations
- We propose an age-dependent conceptual model for sub-slab mantle dynamics

Supporting Information:
- Readme
- Table S1
- Figure S1
- Figure S2

Correspondence to:
C. Lynner,
colton.lynner@yale.edu

Citation:
Lynner, C., and M. D. Long (2014), Testing models of sub-slab anisotropy using a global compilation of source-side shear wave splitting data, *J. Geophys. Res. Solid Earth*, *119*, doi:10.1002/2014JB010983.

Received 24 JAN 2014
Accepted 31 AUG 2014
Accepted article online 4 SEP 2014

Testing models of sub-slab anisotropy using a global compilation of source-side shear wave splitting data

Colton Lynner[1] and Maureen D. Long[1]

[1]Department of Geology and Geophysics, Yale University, New Haven, Connecticut, USA

Abstract Recently, a number of source-side shear wave splitting measurements that directly constrain anisotropy in the upper mantle beneath subducting slabs have been published. Such measurements have yielded an observational foundation on which to base our understanding of the dynamics of the sub-slab mantle. Here we compile measurements from recent studies of source-side splitting beneath slabs that employ identical measurement and processing techniques. We use this compilation to test the predictions of a number of recently proposed conceptual models for the dynamics of the sub-slab mantle, including those that invoke three-dimensional return flow beneath slabs, strong radial anisotropy in suboceanic asthenosphere that is entrained via subduction, and a model based on the correlation between sub-slab splitting behavior and the age of the subducting lithosphere. We find that a model in which fast splitting directions are determined by slab age matches the observations better than either the 3-D return flow or radial anisotropic models. Based on this observation, we propose that the sub-slab mantle is characterized by two distinct anisotropic and mantle flow regimes. Beneath younger lithosphere (<95 Ma), we propose that the sub-slab mantle is characterized by 2-D entrained flow resulting in an entrained mantle layer. Beneath older lithosphere (>95 Ma), the entrained layer is thin and effectively serves as decoupling layer; the dynamics of the sub-slab region beneath old lithosphere is therefore dominated by three-dimensional return flow. This variation in the amount of mechanical coupling may be facilitated by the onset of small-scale convection beneath older lithosphere.

1. Introduction

Subduction zones are vital to our understanding of plate tectonics and mantle circulation, yet our grasp of many aspects of subduction dynamics remains poor; this is particularly true for the sub-slab mantle. Our most direct observational constraints on the dynamics of the sub-slab mantle come from measurements of seismic anisotropy [e.g., *Long*, 2013, and references therein]. Seismic anisotropy in the Earth's upper mantle arises from the tendency of olivine, the dominant upper mantle mineral, to develop a lattice-preferred orientation (LPO) in regions where dislocation creep is the dominant deformation mechanism [e.g., *Karato et al.*, 2008]. Shear wave splitting measurements can therefore be used to infer patterns of mantle flow, as typical olivine LPO fabrics are such that the seismically fast axes of the crystals tend to align with the direction of maximum extensional strain [e.g., *Karato et al.*, 2008]. When shear waves encounter an anisotropic medium, they split into fast and slow polarized waves [e.g., *Vinnik et al.*, 1989; *Silver and Chan*, 1991] and the polarization of these waves, along with the delay time between them, can be measured. The orientation of the fast wave, known as the fast splitting direction (ϕ), contains information about the strain geometry and the delay time (δt) between them contains information about the strength of anisotropy and/or the thickness of the anisotropic layer.

A common technique for isolating the contribution to shear wave splitting from anisotropy in the volume of mantle directly beneath a subducting slab involves measuring the splitting of SK(K)S phases arriving at seismic stations located above a subduction zone and applying a correction for the effect of anisotropy in the mantle wedge [e.g., *Long and Silver*, 2009; *Abt et al.*, 2010]. While this approach provides a first-order picture of anisotropy beneath slabs, it is problematic when trying to place detailed constraints on sub-slab anisotropy. Measurements using this method are limited by the (often sparse) location of seismic instrumentation, which results in poor lateral and depth sampling of the sub-slab mantle. Another shortcoming is that shear wave splitting from SK(K)S phases reflects the integrated effect of anisotropy along the entire (receiver side)

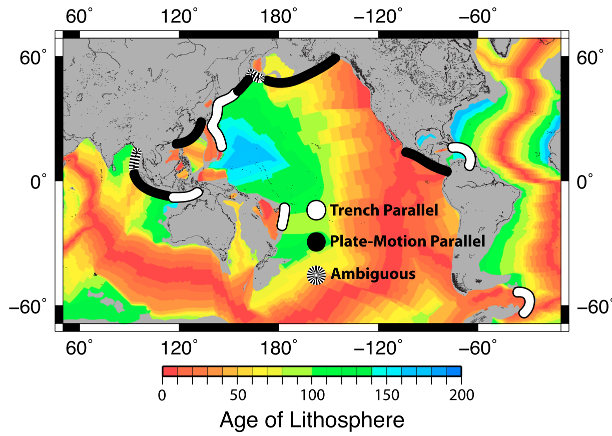

Figure 1. Schematic view of the fast directions of source-side shear wave splitting for all of the regions used in this study. The highlighted color represents the most commonly observed fast direction for different subduction segments, with white corresponding to trench-parallel fast directions and black to plate motion parallel splitting directions. The background is color coded to the age of the oceanic lithosphere from *Müller et al*. [2008b]. A general correlation is apparent between trench-parallel fast directions and older subducting lithosphere, while plate motion-parallel fast directions correlate with younger plate ages.

raypath. This means that each measurement reflects a combined effect of anisotropic signal from the sub-slab mantle, the subducting slab, the mantle wedge, and the overriding plate, making it very difficult to isolate the contribution beneath the slab. While corrections for wedge anisotropy based on local S splitting studies can be applied, these corrections are inexact, as anisotropy in the mantle wedge is usually very complex [e.g., *Wirth and Long*, 2012; *McCormack et al*., 2013; *Long and Wirth*, 2013].

An alternative method for measuring sub-slab anisotropy utilizes the so-called source-side shear wave splitting technique [e.g., *Vinnik and Kind*, 1993; *Russo and Silver*, 1994; *Müller et al*., 2008a; *Russo*, 2009; *Russo et al*., 2010; *Foley and Long*, 2011; *Di Leo et al*., 2012; *Lynner and Long*, 2013, 2014], which measures splitting of teleseismic S phases originating from earthquakes in subducting slabs. A major limitation of this technique is that anisotropy beneath the receiver must be correctly accounted for. In our previous source-side splitting studies [*Foley and Long*, 2011; *Lynner and Long*, 2013, 2014] compiled here, we restricted our analysis to seismic stations for which the upper mantle anisotropy has been well characterized and exhibits only the simplest possible splitting patterns, corresponding to either an apparently isotropic upper mantle or a single flat laying anisotropic layer. (Examples of SK(K)S splitting patterns at such stations can be found in *Foley and Long* [2011] and *Lynner and Long* [2013, 2014]). Strict adherence to these criteria leads to high-quality data sets with minimal contamination from anisotropy beneath the receiver. This method provides direct constraints on anisotropy beneath subducting slabs while avoiding the complexities of the mantle wedge; additionally, it can provide detailed information about the variation of anisotropy both with depth and along strike (see *Lynner and Long* [2013] for additional discussion of the source-side splitting method).

A puzzling observation that has emerged from recent studies of shear wave splitting beneath subducting slabs is that the simplest model for sub-slab mantle dynamics, which invokes two-dimensional entrained mantle flow due to the motion of the overriding plate and simple (A-, C-, or E-type) olivine LPO fabrics, does not correctly predict splitting observations in many subduction zones worldwide. Specifically, this simple model would predict generally plate motion-parallel fast shear wave splitting directions. Overall, however, global sub-slab splitting data sets reveal a mix of trench-parallel, trench oblique, and plate motion-parallel (referring to the motion of the lower plate relative to the upper plate) fast splitting directions [e.g., *Peyton et al*., 2001; *Long and Silver*, 2008, 2009; *Foley and Long*, 2011; *Di Leo et al*., 2012; *Lynner and Long*, 2013, 2014]. This rich variety of observations necessitates a model for sub-slab mantle dynamics and/or anisotropic fabrics that is more complex than a simple single layer of entrained mantle beneath a subducting slab with simple olivine LPO.

Several different models have been proposed to explain sub-slab observations of seismic anisotropy, including 3-D return flow with a strong trench-parallel component [e.g., *Russo and Silver*, 1994; *Long and Silver*, 2008, 2009], aligned serpentinized or fluid-filled cracks within slabs [*Faccenda et al*., 2008; *Healy et al*., 2009], B-type olivine fabric in the sub-slab mantle [*Jung et al*., 2009], and a layer of entrained asthenosphere with strong radial anisotropy beneath slabs [*Song and Kawakatsu*, 2012, 2013]. In addition to these proposed models, we recently documented sub-slab fast splitting directions for circum-Pacific subduction zones that correlate well with the age of the subducting lithosphere (Figure 1), leading us to propose a conceptual model in which sub-slab mantle anisotropy is controlled by slab age [*Lynner and Long*, 2014] and adding to the list of possible models which explain patterns of sub-slab anisotropy. In order to discriminate among

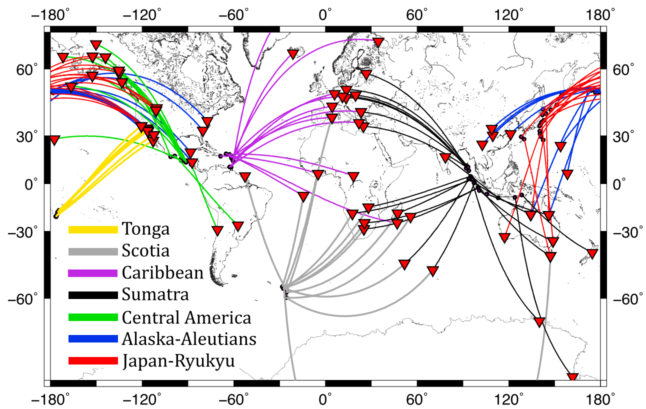

Figure 2. Map of all seismic stations at which source-side splitting measurements in the compilation were made. Great circle paths connect seismic stations to subduction zones where those stations were used to constrain the sub-slab anisotropy from the studies of *Foley and Long* [2011] and *Lynner and Long* [2013, 2014]. Yellow, green, blue, and red lines connect stations to earthquake source regions in the Pacific (Tonga, Central America, Alaska-Aleutians, and Japan-Ryukyu, respectively), while gray, purple, and black lines connect stations to earthquake source regions in Scotia, the Caribbean, and Sumatra, respectively.

these models, detailed shear wave splitting data sets with good spatial and depth coverage that utilize raypaths with a range of azimuths and incidence angles are needed. In this study, we compile several recent source-side shear wave splitting observations [*Foley and Long*, 2011; *Lynner and Long*, 2013, 2014] into one data set against which we can test the predictions made by each conceptual model of sub-slab anisotropy. All sub-slab observations in this compilation were made using identical processing and measurement techniques. Specifically, we compile observations from the Tonga, Caribbean, Scotia, Alaska-Aleutians, Central America, Kurile, Northern Honshu, Izu-Bonin, Ryukyu, and Sumatra subduction zones (Figure 2).

Using this compiled data set, we focus on testing three plausible models for sub-slab anisotropy: the three-dimensional return flow model [*Russo and Silver*, 1994; *Long and Silver*, 2008, 2009], the entrained radial anisotropy model of *Song and Kawakatsu* [2012, 2013], and the age-dependent model suggested by *Lynner and Long* [2014], as these three models are the most consistent with the first-order observations made by source-side splitting studies. The predictions of two additional models, the B-type olivine model of *Jung et al*. [2009] and the serpentinized slab model [*Faccenda et al*., 2008], are not considered to be consistent with first-order aspects of the source-side splitting data set, so we have not tested these models in detail. Specifically, the *Jung et al*. [2009] model proposes a pressure-induced transition to B-type olivine at depths greater than ~90 km, which would change by 90° the relationship between strain and fast splitting directions. No such transition in fast splitting direction with event depth has been observed [*Foley and Long*, 2011; *Lynner and Long*, 2013, 2014]. The serpentinized slab model proposed by *Faccenda et al*. [2008] invokes aligned, serpentinized cracks in the subducting slab leading to strong trench-parallel splitting. While this mechanism may play a role in the overall anisotropic signature, it is an unlikely candidate to explain global patterns of source-side splitting, as source-side studies have shown consistent splitting at depths of ~100 km and greater [e.g., *Foley and Long*, 2011; *Lynner and Long*, 2013, 2014], which is far below the stability field for antigorite, the most likely serpentine mineral to be present [*Ulmer and Trommsdorff*, 1995].

We focus our attention, therefore, on the three-dimensional return flow model [*Russo and Silver*, 1994; *Long and Silver*, 2008, 2009], the strong radial anisotropy model of *Song and Kawakatsu* [2012, 2013] (Figure 2), and our recently proposed age-dependent model [*Lynner and Long*, 2014]. To first order, the 3-D return flow model makes a general prediction of trench-parallel fast splitting directions in the sub-slab mantle for systems undergoing trench migration, with weak sub-slab anisotropy for systems with nearly stationary trenches that may not have accumulated significant strain in the sub-slab mantle [e.g., *Faccenda and Capitanio*, 2012]. This model invokes the rollback motion of the subducting slab as a cause of three-dimensional return flow, in turn leading to a complex flow field directly beneath the slab with a dominant component that is parallel to the trench (Figure 3).

The strong radial anisotropy model of *Song and Kawakatsu* [2012, 2013] (Figure 3) proposes that the asthenospheric mantle beneath oceanic lithosphere is characterized by both azimuthal and radial anisotropy in a specific combination (relatively strong radial anisotropy and relatively weak azimuthal anisotropy). In this model, the downgoing plate entrains the mantle beneath it, as viscous coupling between the slab and the subjacent mantle results in asthenospheric mantle that is dragged downward with the slab. As the dip of the slab increases, the radial anisotropic component of the sub-slab anisotropy will have a

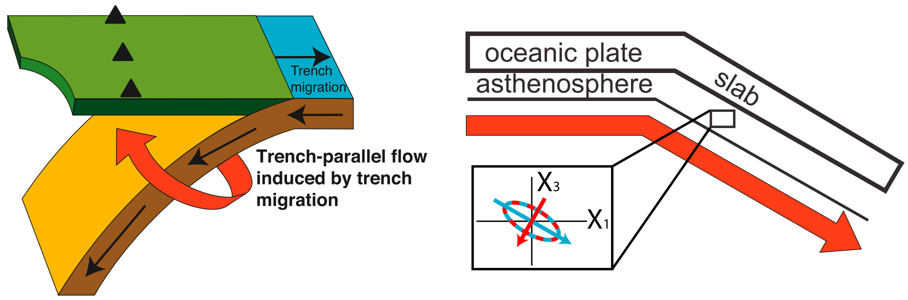

Figure 3. Conceptual diagrams of (left) the 3-D return flow model of *Russo and Silver* [1994] and *Long and Silver* [2008, 2009] and (right) the strong radial anisotropy model of *Song and Kawakatsu* [2012, 2013]. The 3-D return flow model is characterized by flow in the sub-slab mantle that has a strong trench-parallel component, induced by the rollback motion of the slab. The strong radial anisotropy model is characterized by entrained mantle flow beneath a subducting slab; in this model, the asthenospheric mantle beneath subducting plates is characterized by a strong radial anisotropy and a somewhat weaker azimuthal anisotropy. Specifically (see inset diagram), the fast direction of azimuthal anisotropy (blue arrow) is oriented parallel to the flow direction, while the slow axis of radial anisotropy (red arrow) is oriented perpendicular to the dip of the slab above it. Modified from *Long and Silver* [2008] and *Song and Kawakatsu* [2012].

stronger effect on (nearly) vertically incident shear waves (e.g., SKS) than the azimuthal component, leading to trench-parallel fast splitting directions for some raypath geometries. The specific combination of radial and azimuthal anisotropy proposed by *Song and Kawakatsu* [2012, 2013] makes predictions about how shear wave splitting should vary with incidence angle and event-station azimuth.

Lastly, our recently proposed age-dependent model [*Lynner and Long*, 2014] is based on the observation that sub-slab fast splitting directions seem to correlate with the age of the downgoing lithospheric plate. In *Lynner and Long* [2014], we measured splitting beneath the circum-Pacific and Sumatra slabs, examined correlations among splitting parameters and many different subduction-related parameters (e.g., slab dip and convergence velocity slab width), and found that only age of the subducting slab correlated well with splitting. Specifically, we observed that younger slabs (lithospheric age $<$ 95 Ma) generally exhibit plate motion-parallel fast directions, while older slabs generally exhibit trench-parallel fast orientations (Figure 1). Based on this observation, we posit that older slabs (lithospheric age $>$ 95 Ma) are sufficiently decoupled from the mantle beneath them such that the sub-slab mantle undergoes 3-D return flow, while younger slabs remain relatively well coupled to the subjacent mantle and entrain a relatively thick (~200 km) layer of mantle beneath them. To first order, this model predicts trench-parallel fast directions beneath older subducting slabs as long as trench migration is sufficient to induce 3-D return flow, and plate motion-parallel splitting beneath younger slabs as the overriding slab entrains the subjacent mantle. This model, as well as the 3-D return flow model [*Russo and Silver*, 1994; *Long and Silver*, 2008, 2009], assumes that the upper mantle is characterized by typical olivine LPO fabrics (A, C, or E type).

2. Data: A Uniform Compilation of Sub-Slab Splitting Measurements

In order to test the various sub-slab anisotropy models, we have compiled a uniform data set of sub-slab shear wave splitting measurements for the Tonga, Caribbean, Scotia, Alaska-Aleutians, Central America, Kurile, Northern Honshu, Izu-Bonin, Ryukyu, and Sumatra subduction zones (Figure 2), based on the work of *Foley and Long* [2011] and *Lynner and Long* [2013, 2014]. Although source-side measurements for other subduction systems are available in the literature (e.g., South America [*Russo and Silver*, 1994; *Russo et al.*, 2010; *Eakin and Long*, 2013], Cascadia [*Russo*, 2009], and Indonesia [*Di Leo et al.*, 2012]), we have chosen to focus on measurements made using a uniform set of station selection criteria, raypath geometry selection criteria, preprocessing methods, frequency content, measurement methodologies, and receiver-side correction procedure. (Station correction values and examples of SK(K)S splitting used to constrain receiver-side anisotropy can be found in each study from which observations were compiled; an example of the receiver-side correction procedure can be found in *Lynner and Long* [2014], and a map of all the stations used in this compilation can be seen in Figure 2.) This allows for consistency among the different studies and also follows a stringent set of criteria for station selection (as detailed in *Lynner and Long* [2013]). Our process for station selection and receiver-side anisotropy corrections circumvents some of the possible problems with improper characterization of upper mantle anisotropy beneath the receivers, as this can result in substantial errors using the source-side technique [*Lynner and Long*, 2013, 2014]. We examined SK(K)S splitting at every station, and, in general, errors on individual splitting measurements used to constrain receiver-side anisotropy are up to ~15° and 0.5 s for fast direction and delay time, respectively. Different stations have different backazimuthal coverage, but when choosing stations we required consistency (within ~10° for fast direction, which is less than error for a typical measurement) among several backazimuthal swaths. Therefore, the effect of receiver-side anisotropy corrections on estimates of sub-slab splitting should be minimal. We also applied more stringent quality control criteria to the measurements of *Foley and Long* [2011] and *Lynner and Long* [2013], excluding some measurements for the Tonga, Caribbean, and Scotia data sets that did not match the criteria used by *Lynner and Long* [2014].

Here we briefly summarize the observations from our previous studies for each subduction system, Figure 2. The Tonga subduction zone is characterized by nearly trench-parallel sub-slab fast splitting directions; this pattern persists for earthquakes down to transition zone depths (as deep as ~650 km), although we only use measurements corresponding to event depths less than 250 km in this study, as our focus is on the upper mantle. The Tonga study of *Foley and Long* [2011] is limited in backazimuthal extent, as all of the seismic stations used are located in western North America (near the Baja Peninsula). The highly curved Caribbean subduction zone exhibits trench-parallel splitting throughout the northern portion of the trench, while in the southernmost region, plate motion-parallel splitting is seen [*Lynner and Long*, 2013]. The Scotia subduction zone is marked by scattered sub-slab splitting directions, varying from plate motion-parallel to trench-parallel ϕ, with the dominant direction being trench parallel [*Lynner and Long*, 2013; see also *Müller et al*., 2008a]. The Central America, Alaska-Aleutians, and Ryukyu subduction zones are all characterized by dominantly plate motion-parallel splitting directions, although the fast directions beneath Alaska are highly scattered [*Lynner and Long*, 2014]. Northern Honshu and Izu-Bonin both are dominated by trench-parallel splitting [*Lynner and Long*, 2014]. Finally, the Kurile and Sumatra subduction systems exhibit along-strike variations, with regions of both trench-parallel and plate motion-parallel ϕ [*Lynner and Long*, 2014]. A sketch of the dominant fast splitting directions in our compilation is shown in Figure 1.

3. Methods and Model Testing

A key issue in the interpretation of the sub-slab splitting data set is whether the measurements primarily reflect frozen-in anisotropy within the slab itself, flow in the sub-slab mantle, or a combination of the two. In this study we assume that the observations are solely due to anisotropy in the sub-slab upper mantle; we neglect contributions from other parts of the system, such as the slab itself. There are three lines of evidence to justify this assumption, as discussed in detail in *Lynner and Long* [2014]. First, our selection of stations that lie in an updip direction means that raypaths are chosen to minimize the raypath length within the slab (typically less than ~100 km even for the oldest slabs and less for younger slabs) relative to the raypath length in the sub-slab mantle (typically several hundred kilometers). Second, we examined many different events that yielded measurements at multiple stations and generally obtained very similar results for both fast direction and delay time. For many of these examples, the path length through the slab varies among the different raypaths, but the splitting measurements do not, suggesting that the primary contribution comes from (relatively homogeneous) anisotropy in the sub-slab mantle. Third, and perhaps most convincingly, in two regions (Sumatra and Kurile) we have documented an abrupt change in fast splitting direction along strike [*Lynner and Long*, 2014]. While we would expect the properties of the oceanic lithosphere, particularly its thickness, to vary with age, we would expect these variations to be smooth. Thus, any variations in anisotropic properties of the slab itself due to frozen-in lithospheric anisotropy (or acquired via deformation during subduction) should also vary smoothly. It is difficult to reconcile the abrupt change in splitting we observe with the gradual nature of the acquisition of frozen-in anisotropy in the lithosphere. Therefore, our interpretation of the sub-slab measurements is that slab anisotropy may make a modest contribution to the observed splitting but is not likely to be the primary source. Our forward modeling approach thus incorporates only anisotropy due to sub-slab mantle flow; we acknowledge, however, that it is not possible to completely rule out some contribution from slab anisotropy.

In order to test quantitatively the three different models for sub-slab anisotropy, we make a series of assumptions about elastic tensors and their orientations with respect to the slab geometry for each model.

We then use a ray theoretical approximation to calculate the predicted splitting for each (nonnull) direct S raypath in our data set. These calculations require knowledge of the takeoff angle and azimuth of the downgoing *S* wave beneath the slab (derived from the station and event locations), the local slab dip, the motion of the subducting plate, the local orientation of the trench, and the local age of the subducting lithosphere. We used the TauP program [*Crotwell et al*., 1999] with the isap91 Earth model [*Kennett and Engdahl*, 1991] to calculate the paths of the downgoing *S* waves. Straight line approximations from the event location to the pierce point at the 410-discontinuity were used to calculate the takeoff angles for each S ray in the splitting data set. Although a straight line approximation for the raypath is imperfect, it should make little difference in our calculations, as the angle between the ray propagation direction and the vertical is not expected to change much in the upper mantle for the rays in our data set.

Slab dips at relevant depths were obtained from the compilation of *Lallemand et al*. [2005]. *Lallemand et al*. [2005] report dips for the shallow (<125 km) and deep (>125 km) portions of slabs. Since we restrict event depths in the compiled data set to those shallower than 250 km, the majority of events correspond to depths consistent with the shallow dip reported in *Lallemand et al*. [2005], but for events deeper than 125 km, we use the deeper dip estimates. The motions of the subducting slabs were calculated from the MORVEL plate model [*DeMets et al*., 2010]. There is much debate about the correct reference frame when evaluating splitting measurements relative to the mantle or to subducting slabs [e.g., *Long and Silver*, 2009]. Here we have chosen to evaluate downgoing plate motions in the reference frame of the upper plate, as this is a natural reference frame in which to evaluate subducting plate motion. *Lynner and Long* [2014] compared downgoing plate motion vectors for this reference frame to those calculated in a no-net-rotation reference frame and a Pacific hot spot reference frame for many of the subduction systems examined here and found that the differences were generally minor. The local orientation of the trench was calculated by examining the orientation of the 50 km contours of the subducting slabs in the global slab model of *Gudmundsson and Sambridge* [1998]. The azimuth of the rays is set by the event-station geometry.

We evaluated the age of the subducting lithosphere at a depth of 100 km in the subduction zone from the slab age model of *Cruciani et al*. [2005]. *Cruciani et al*. [2005] did not, however, calculate slab age as a function of depth for systems in which isochrons of seafloor lithospheric age are roughly parallel to the motion of the subducting slab. In this case, the lithospheric ages likely vary minimally with depth, although faulting in the subducting lithosphere may alter this relationship (and is very poorly known). In regions where there is no calculation for lithospheric age at depth in the *Cruciani et al*. [2005] study, we use the seafloor age at the trench, from the compilation of *Heuret and Lallemand* [2005].

For each of the three models considered, we use an appropriate approximation for the elasticity of the sub-slab mantle as follows. For the strong radial anisotropy model, we use the elastic tensor proposed by *Song and Kawakatsu* [2012] to represent the anisotropy of the sub-slab mantle. We assume that the anisotropic medium has an azimuthal orientation and dip controlled by the downgoing plate motion and the slab dip, respectively, and rotate the elastic tensor accordingly for the local slab geometry (Figure 2), taking into account the obliquity angle for systems with oblique convergence.

The 3-D return flow model [*Russo and Silver*, 1994; *Long and Silver*, 2008, 2009] invokes generally trench-parallel sub-slab finite strains induced by trench rollback (Figure 3). In real subduction systems, a three-dimensional flow field is likely to have substantial complications (e.g., complex flow around the edges of the slab and perturbations to the flow field due to complex slab morphology), and for realistic three-dimensional slab rollback models, the distribution of finite strain in the sub-slab mantle is also likely to be fairly complicated [e.g., *Buttles and Olson*, 1998; *Faccenda and Capitanio*, 2012; *Paczkowski et al*., 2014]. In this study, we approximate this complexity with a single layer of anisotropy with trench-parallel finite extension directions. This is a significant simplification, but here we aim to capture only the first-order characteristics of this complex strain field. A detailed comparison between the predictions of geodynamical models with realistic slab geometries and sub-slab splitting observations is beyond the scope of this paper. Instead, we make a simplified assumption that 3-D return flow induced by trench rollback will result in generally trench-parallel sub-slab strains, which we approximate by assuming that the fast axis of anisotropy locally aligns with the trench strike in the horizontal plane. We represent the elastic properties of the mantle using the elastic tensor from *Chevrot and van der Hilst* [2003], which invokes a transversely isotropic (that is, hexagonal) approximation for upper mantle elasticity. We further assume that every subduction system considered is undergoing some degree of trench migration

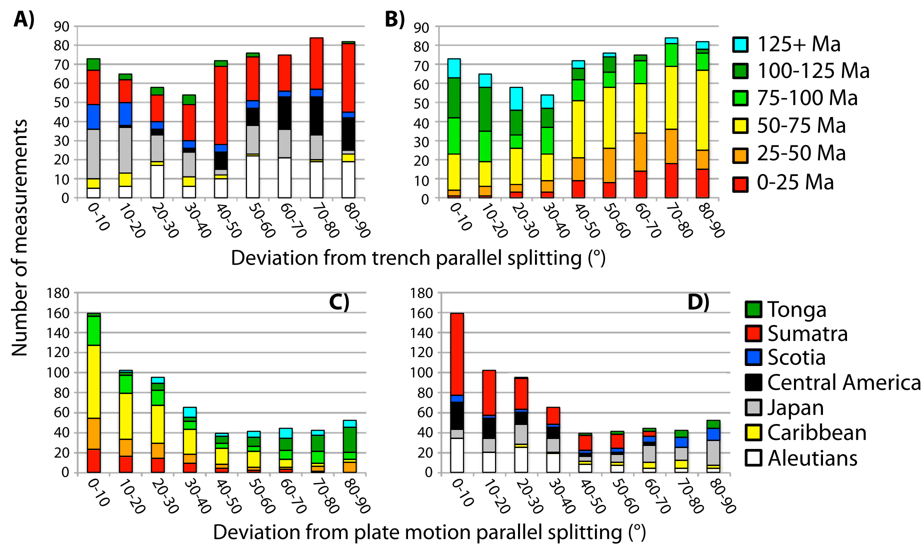

Figure 4. Histogram plots of measured fast splitting directions from our quasi-global source-side splitting data set, derived from the studies of *Foley and Long* [2011], *Lynner and Long* [2013], and *Lynner and Long* [2014]. Individual panels show (a and b) the deviation between the measured fast direction and the local strike of the trench and (c and d) the deviation between the fast direction and the local motion of the downgoing. In Figures 4a and 4d, the measurements are color coded according to geographic region, while in Figures 4b and 4c the measurements are color coded according to the age of the subducting lithosphere (legends are on the right). These histograms confirm a primary finding from our earlier work [*Lynner and Long*, 2014]: there is a correlation between fast splitting direction and age of the subducting lithosphere, with old slab ages correlating with trench-parallel ϕ and young ages correlating with plate motion-parallel ϕ.

and has a slab geometry that is suitable for inducing some degree of 3-D return flow. These assumptions represent a highly simplified view of the three-dimensional sub-slab flow. A more realistic geodynamical modeling study, which takes into account actual trench migration rates and background mantle flow and calculates the distribution of finite strain directions for different subduction systems, has recently been carried out [*Paczkowski et al.*, 2014]. In this study, however, we use a simplified view of trench-parallel sub-slab flow as a first approximation.

For the age-dependent model, we use the observations of *Lynner and Long* [2014] as a guide; our previous study estimated an age of ~95 Ma at the trench at which a transition from plate motion-parallel fast directions to trench-parallel fast directions is generally observed (Figure 1). This estimate is borne out by an examination of the full quasi-global data set compiled here; Figure 4 shows histograms of all measured fast splitting directions for our compilation as a function of subduction region and plate age. Through examination of fast splitting directions from *Foley and Long* [2011] and *Lynner and Long* [2013, 2014] and different lithospheric ages (90 Ma, 95 Ma, and 100 Ma), we find that the transition in fast splitting directions best corresponds to a lithospheric age of 95 Ma. In our model predictions, therefore, for systems with a lithospheric age less than 95 Ma, we assumed that the fast axis of anisotropy aligns with the motion of the downgoing plate (as constrained by the slab dip and plate motion vector) as would be expected for simple entrained two-dimensional flow. The hexagonal elastic tensor of *Chevrot and van der Hilst* [2003] was then rotated according to the slab dip, downgoing plate motion, and local trench strike to approximate entrained flow. For systems with a lithospheric age greater than 95 Ma, we assumed that the fast axis of anisotropy lies in the horizontal plane and is aligned with the local trench strike, following the same procedure as for the 3-D return flow model.

Splitting predictions for each S raypath for each of the three models were calculated using the MSAT software package [*Walker and Wookey*, 2012], which predicts splitting parameters by solving the Christoffel equation for a uniform anisotropic volume. We focused only on predicting the fast splitting directions and did not attempt to predict the delay times, for several reasons. First, from an observational point of view, δt values are generally less well constrained than ϕ values. Second, there is little variability in average delay times between different regions or within the same region [e.g., *Lynner and Long*, 2014]. Finally, because there is a direct

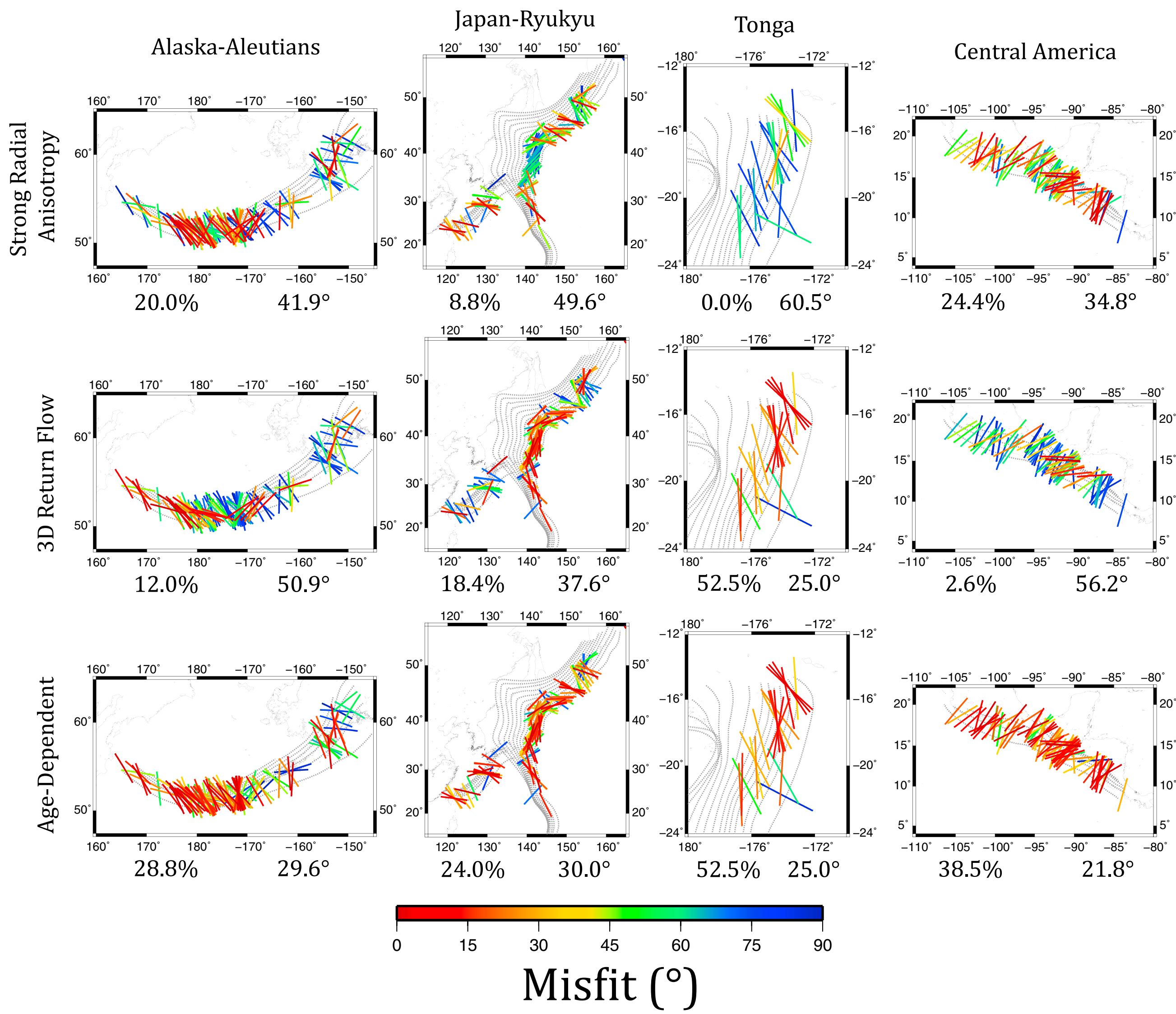

Figure 5. Deviations between predicted and observed fast splitting directions for (top) the entrained radial anisotropy model, (middle) the 3-D return flow model, and (bottom) the age-dependent model. For each raypath in the data set, we plot the observed fast splitting direction (thin bars), with the orientation of the bars corresponding to the observed ϕ and the color of the bar corresponding to the difference between the model prediction and the observation in degrees (see color bar at bottom). From left to right, we show predictions for the Alaska-Aleutians, the Japan-Ryukyu system, Tonga, and Central America. Beneath each panel, we show the average misfit (in degrees, on the right) and the percentage of splitting predictions that fall within the 2σ errors of the corresponding measurement (on the left) for the specific region and model being tested.

tradeoff between layer thickness and anisotropic strength, predictions of absolute delay times are not meaningful. We therefore focus on predicting the variability in the measured fast directions.

4. Results

For each model under consideration, we generated predictions of fast splitting directions for each of the 623 individual nonnull source-side shear wave splitting measurements in our compiled data set. These predictions are shown in Figures 5, 6, S1, and S2 in the supporting information (with different plotting conventions). We also show examples of the model predictions for the *Song and Kawakatsu* [2012, 2013] model, the 3-D return flow model [*Russo and Silver*, 1994; *Long and Silver*, 2008, 2009], and the age-dependent model [*Lynner and Long*, 2014] as a function of azimuth and takeoff angle for several selected regions in Figures 7–9. We evaluate the fits between the model predictions and the splitting observations both

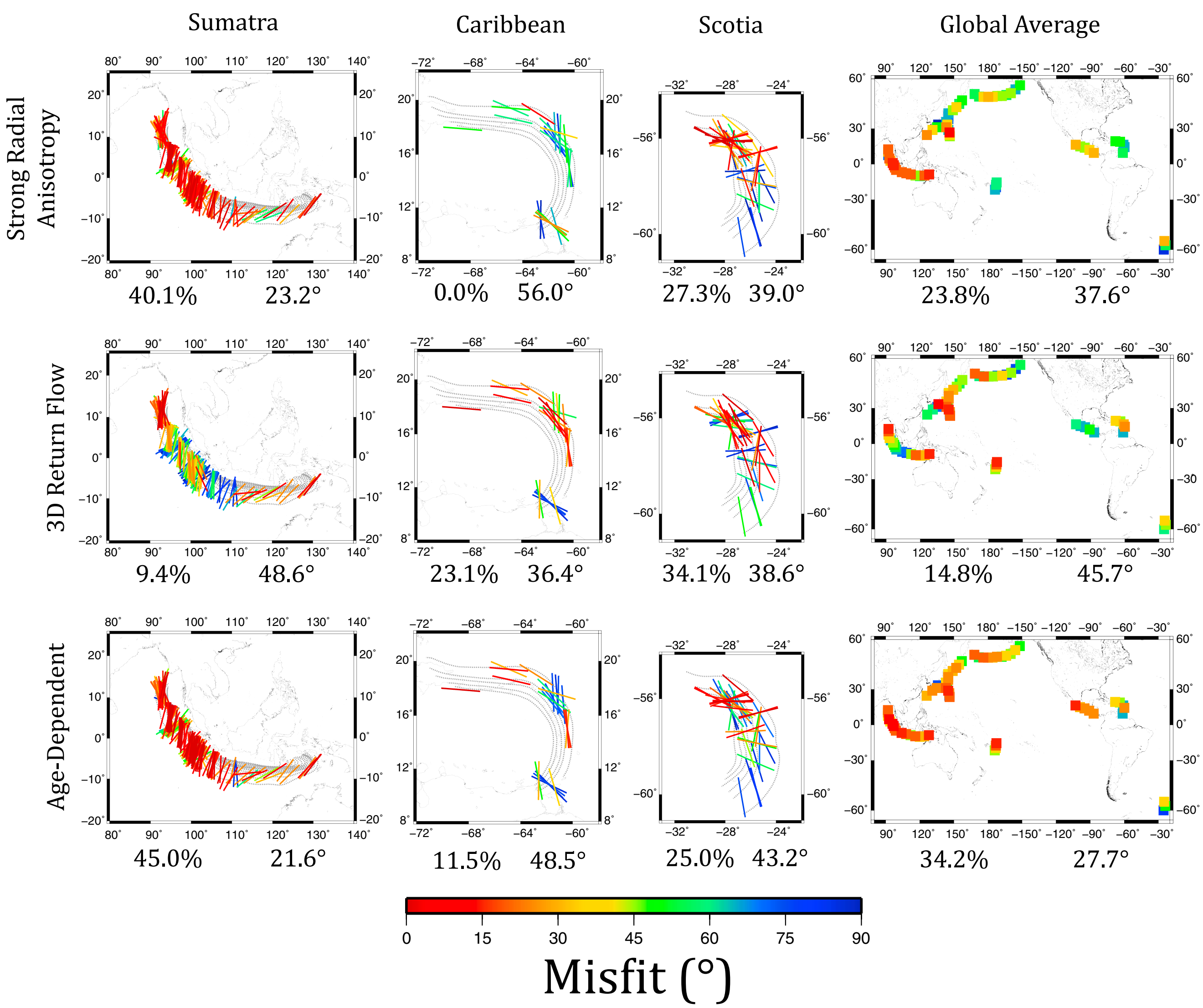

Figure 6. Deviations between predicted and observed fast splitting directions for (top) the entrained radial anisotropy model, (middle) the 3-D return flow model, and (bottom) the age-dependent model. From left to right, we show predictions for the Sumatra, Caribbean, and Scotia subduction zones, as well as for the global data set. The plotting conventions for the Caribbean, Scotia, and Sumatra regions are as in Figure 5. For the global map (far right), we plot symbols color coded by the average deviation between the model predictions and observations for individual subduction segments.

qualitatively (via visual inspection) and quantitatively, with two different criteria to evaluate model fit. The first criterion is the absolute value of the difference in fast direction between the measurement and the model prediction in degrees (referred to here as misfit). We calculated average misfit values for individual subduction systems for each model, as described below. The second is the percentage of model predictions that fall within the 2σ errors of their corresponding measurement (referred to as data match) for each region. We did not apply any weighting scheme in applying our model fit criteria and report simple nonweighted averages throughout this study. Predicted fast splitting directions for each direct S raypath for each model considered, measured splitting parameters with 2σ errors, station information, source locations, and variables used in making the predictions for the various models (e.g., slab dip, plate motions, and trench strike) can be found in Table S1.

First, we examine the circum-Pacific subduction zones (Figure 5), namely, the Kurile, Northern Honshu, Izu-Bonin, and Ryukyu regions (which we collectively refer to as the Japan-Ryukyu system), Central America, Alaska-Aleutians, and Tonga. Beneath the Japan-Ryukyu system, the age-dependent anisotropic model matches the data best, with an average misfit of 30.0° and with 24.0% of the predictions matching the

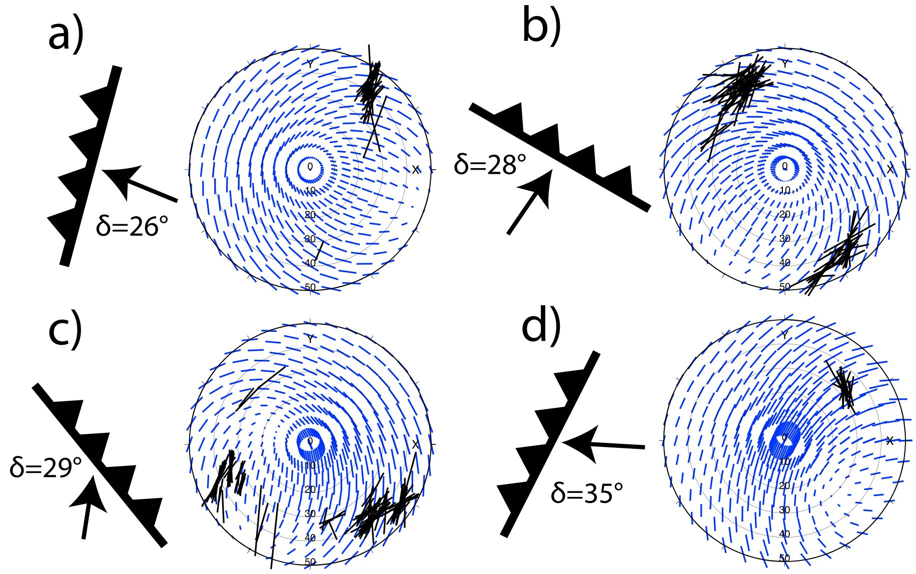

Figure 7. Model predictions (blue bars) and observations (black bars) for the strong radial anisotropy model for the (a) Northern Honshu, (b) Central America, (c) Sumatra, and (d) Tonga subduction zones, as a function of takeoff angle and event-to-station azimuth. The orientation and length of the bars correspond to fast direction and delay time, respectively. The distance from the center of the plot corresponds to the takeoff angle of the ray, while azimuth corresponds to event-to-station azimuth. Next to each plot is a schematic of the local orientation of the trench and the motion of the subducting plate with the dip of the slab (δ) used to generate the predictions. For Northern Honshu, we show measurements located between 35.5°N and 40.3°; for Central America, we include all the measurements; for Sumatra, we show measurements between 5°S and 5°N; for Tonga, we show measurements made south of 17.2°S. These geographical bounds were chosen to correspond to the regions with relatively straight trench geometries.

observations. Randomly oriented fast directions would match ~16% of the data and would have a misfit of ~45°; our result of an average misfit of 30.0° and 24.0% of observations matching the predictions is therefore statistically significant ($p < 0.05$) when compared to a null hypothesis in which all fast directions are randomly oriented. (In general, misfit values of less than ~38° and data match values greater than ~22% for all regions tested are statistically significant ($p < 0.05$) when compared to randomly oriented fast directions.) Given the amount of scatter in the data and the very simplified assumptions employed in each model, we do not expect to be able match every observation, but our average misfit and data match values allow us to evaluate which models predict the observations better than random chance. The second best fit was the 3-D return flow model, which had an average misfit of 37.6° and matched 18.4% of the data. Lastly, the strong radial anisotropy model matched 8.8% of the data with an average misfit of 49.6°. Visual inspection of the model predictions (Figure 5) reveals that both the age-dependent model and the 3-D return flow model generally match the observations well for the Izu-Bonin, Honshu, and Hokkaido regions. For the Kurile and Ryukyu regions, the age-dependent model generally fits the observations well (although there is scatter in the data), while the 3-D return flow model does not do a good job of predicting the observations. Throughout the Japan-Ryukyu region, the entrained radial anisotropy model generally does not do a good job of fitting the observations. While some observations are predicted well, the majority of observations are predicted poorly.

Beneath Alaska and the Aleutians, we again found that the age-dependent model did the best job of predicting the observations, with an average misfit of 29.6° and an overall data match of 28.8%. The strong radial anisotropy model had the second best fit, with a 41.9° average misfit and a 20.0% data fit, while the 3-D return flow model had the poorest match with values of 50.9° and 12.0%, respectively. Qualitatively, it is clear (Figure 5) that the age-dependent model does a good job of matching observations in the western part of the subduction system, but the fit is less good beneath the eastern part. For both the 3-D return flow model and the entrained radial anisotropy model, there is a mix of well-predicted and poorly predicted fast directions throughout the region. Notably, none of the three models tested do a good job of reproducing the observations beneath Alaska, which are highly scattered and may reflect a contribution from anisotropy within the slab itself [*Lynner and Long*, 2014]. Model predictions for the Central American subduction system

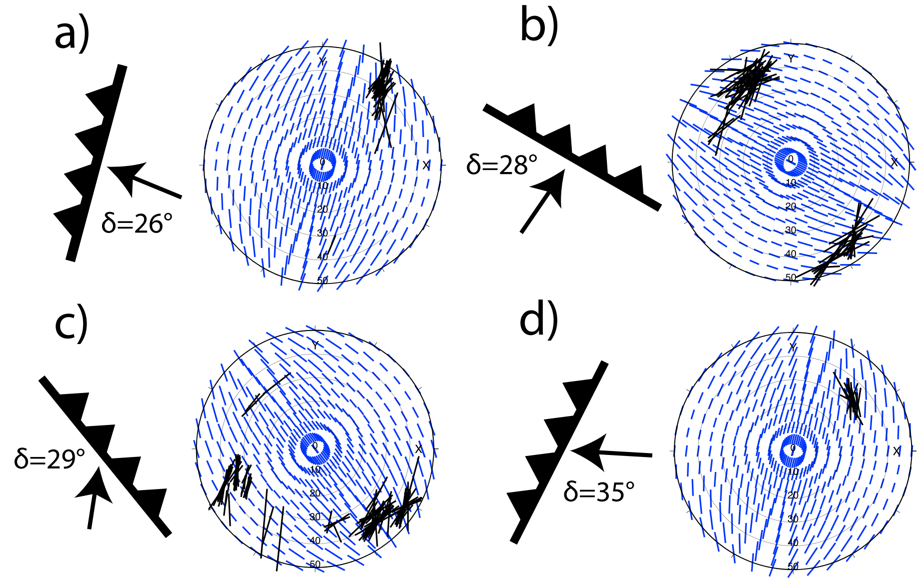

Figure 8. Model predictions (blue bars) and observations (black bars) for the 3-D return flow model for the (a) Northern Honshu, (b) Central America, (c) Sumatra, and (d) Tonga subduction zones, as a function of takeoff angle and event-to-station azimuth plotted following the same plotting conventions as Figure 7.

follow a similar pattern, with the age-dependent model having the best fit (21.8° average misfit and 38.5% data match) and the entrained radial anisotropy model second (34.8° average misfit and 24.4% data match). The 3-D return flow model does a very poor job of matching the observations beneath Central America, with an average misfit of 56.2° and 2.6% of the predicted fast directions falling within the 2σ errors of the corresponding measurement. In map view, the age-dependent model correctly generally predicts the splitting patterns well throughout the subduction system (Figure 5) while the fit is poor throughout the subduction system for the 3-D return flow model and the entrained radial anisotropy model exhibits a mix of those measurements that are fit well and those that are fit poorly.

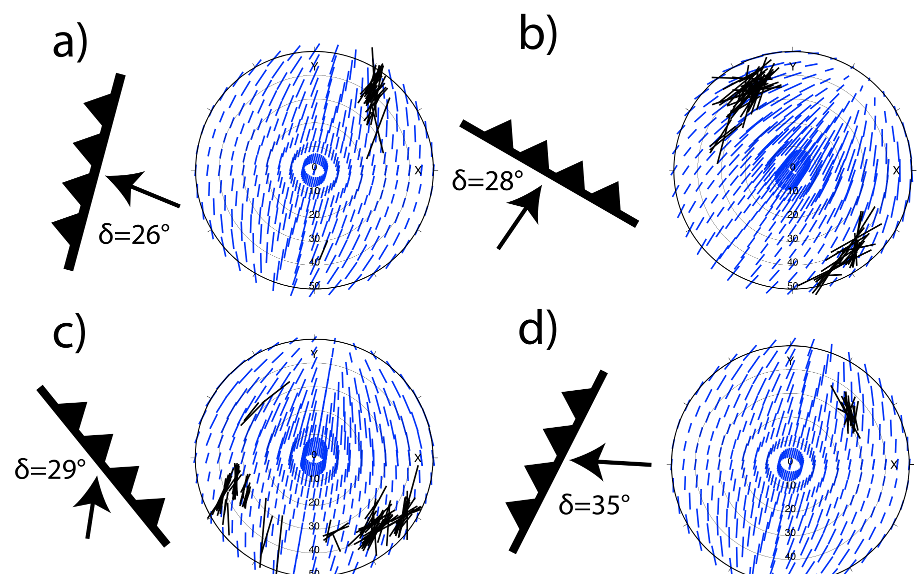

Figure 9. Model predictions (blue bars) and observations (black bars) for the age-dependent model for the (a) Northern Honshu, (b) Central America, (c) Sumatra, and (d) Tonga subduction zones, as a function of takeoff angle and event-to-station azimuth following the same plotting conventions as Figure 7.

Beneath Tonga (Figure 5), all of the splitting measurements come from the northern portion of the subduction zone where old (~110 Ma) lithosphere being subducted, so the 3-D return flow and the age-dependent model make the same predictions. Each of these models fit the observations well, with an average misfit of 25.0° and a data match of 52.2% of the measurements. The strong radial anisotropy model, in contrast, provides a poor fit to the data; this model matched none of the observations and had an average misfit of 60.5°. In map view, the 3-D return flow and age-dependent models seem to do a generally good to fair job of matching the observations, although as in other regions there is scatter in the observations themselves.

Model predictions for the Caribbean, Scotia, and Sumatra subduction zones are shown in Figure 6. The Caribbean subduction system exhibits a complicated geographical distribution of lithospheric ages; for a portion of the subduction zone the lithosphere is older than 95 Ma, but throughout the middle portion (where the majority of measurements were made) the subducting lithosphere is just slightly younger (~94 Ma) than the 95 Ma cutoff we employ in this study for the transition from plate motion-parallel to trench-parallel regimes in the age-dependent model. The best fitting model for the Caribbean is the 3-D return flow model, which has an average misfit of 36.4° and matches 23.1% of the data. The age-dependent model has a misfit value of 48.5° and matches 11.5% of the splitting measurements. The strong radial anisotropy model fails to match any of the observations and has an average misfit of 56.0°. In map view (Figure 6), the 3-D return flow model does a generally good job of predicting fast directions in the northern portion of the subduction zone, where the observed fast directions clearly correlate with the strike of the trench. However, this model fails to predict a group of observations in the southern portion of the subduction zone that exhibit nearly trench-perpendicular fast directions, as do the strong radial anisotropy and age-dependent models. The age-dependent model does a fair job of predicting fast directions in the northernmost portion, but due to the lithospheric age of ~94 Ma in the central region, the model predicts plate motion-parallel fast directions when trench-parallel fast directions are observed.

Beneath Scotia, the 3-D return flow model provides the best fit, with an average misfit of 38.6° and a data match value of 34.1%. In map view (Figure 6), it is clear that the model does a better job of predicting the fast directions in the northern portion of the subduction zone. The strong radial anisotropy model provides a similar misfit (39.0°) and matches 27.3% of the observations, so it performs nearly as well as the 3-D return flow model. The age-dependent model fits the measurements the least well, matching only 25.0% with a misfit of 43.2°. Again, looking at a map view, predictions from all three models do a particularly poor job in the southern portion of the system (it is worth emphasizing again that the Scotia splitting data set has a large amount of scatter in the observed fast directions). Finally, observations beneath the Sumatra subduction system (Figure 6) are best matched by the age-dependent model, which correctly predicts 45.0% of the observations and exhibits an average misfit of 21.6°. The strong radial anisotropy model yields slightly worse misfit and data match values, 23.2° and 40.1%; the 3-D return flow model performs poorly, with an average misfit of 48.6° and a data match of 9.4%.

When all of the subduction zones are considered as a whole, while no one model perfectly predicts the global source-side shear wave splitting data set, the age-dependent model does a better job overall than the other models at predicting the observations. A map view of the average misfit for individual segments of all subduction zones (right panels on Figure 6) reveals that the age-dependent model generally does a good job of fitting the observations for most regions, particularly Sumatra, the Aleutians, the Japan-Ryukyu region, Central America, and Tonga, and only fails in a few specific regions (portions of the Caribbean and much of Scotia). While the 3-D return flow model fits the observations well in certain regions (most of the Caribbean, Scotia, Izu-Bonin-Honshu, Tonga, and the eastern and western edges of Sumatra), there are several regions in which the fit is notably poor (Central America, southern Caribbean, the Aleutians, Ryukyu, and much of Sumatra). The strong radial anisotropy model also does a very good job matching the observed splitting fast directions in many regions (Sumatra, Scotia, and Central America) but does a poor job in others (the Japan-Ryukyu system) and fails to match any of the observations in Tonga or the Caribbean. Our calculated data fit metrics for the entire data set as a whole reveal that the age-dependent model matches 34.2% of the observations globally and has an average misfit of 27.7°. The strong radial anisotropy model had a larger average misfit (37.6°) and matched 23.8% of the data, and the 3-D return flow model matched only 14.8% of the measurements and had the highest average misfit value (45.7°).

5. Discussion

Several broad trends in the model predictions themselves are evident and are helpful in evaluating how well the various models match the observations. It is worth noting that for both the age-dependent and 3-D return flow models, the predicted fast directions for the range of direct S raypaths in this study are generally very close to either the strike of the trench or (for the age-dependent model) the convergence direction. Therefore, the degree of scatter in the predicted fast directions is relatively small for these models. (This is particularly easy to visualize in Figures S1 and S2, which plot the predicted fast splitting direction for each raypath in the data set for each model.) In contrast, the strong radial anisotropy model predicts a strong dependence in predicted fast splitting direction as a function of incidence angle and (most importantly) event-station azimuth. Therefore, this model predicts large and systematic variations in fast directions depending on the event-station geometries of the rays (Figures S1 and S2). This is worth noting because, with the exception of Scotia and the eastern portion of the Alaska-Aleutians, the actual source-side fast splitting directions exhibit less variation in ϕ than generally predicted by the *Song and Kawakatsu* [2012] model.

Another observation worth noting is that none of the models do an especially good job predicting the observed plate motion-parallel fast splitting directions observed beneath the southern portion of the Caribbean subduction zone. We have previously argued [*Lynner and Long*, 2013] that the dynamic behavior of the mantle in this region is constrained by the presence of the deep keel of the South American continental lithosphere. The deep keel may create a barrier that prevents any southward mantle flow, leading to plate motion-parallel stretching (and thus fast splitting directions) beneath the subducting slab. It is worth noting, however, that recently published regionally specific mantle dynamics models which taking into account the slab morphology and the presence of the South American continental lithosphere did not predict our observations well [*Miller and Becker*, 2012]. In any case, such complications were not incorporated into any of our simplified model predictions, which may explain why none of the models tested explain the observations beneath the southern Caribbean very well. This failure highlights the continuing need for regionally specific models that take into account the morphology and kinematics of individual subduction systems. It also raises the possibility that the model parameters used to predict fast splitting directions globally in each model might not be the best parameters for use in individual regions. (For example, the amount of radial anisotropy in the *Song and Kawakatsu* [2012] model or the age at which the transition from trench-parallel to plate motion-parallel fast direction occurs in the age-dependent model may vary slightly between regions.)

We emphasize that we have taken a simplified approach to carrying out splitting predictions for different models in this study, and thus, our conclusions come with some caveats. For example, we have used simplified descriptions of slab morphology and kinematics, and for the 3-D return flow and age-dependent models, we have used a simplified (hexagonal) representation of the elastic tensor. Our evaluation of the 3-D return flow model in particular is highly simplified, in that we have assumed that for the case of subduction with trench migration, the spatial gradients in mantle flow velocity are such that the direction of maximum finite extension (and thus the fast axis of anisotropy) will always align parallel to the local strike of the trench. Finally, we have assumed that all subduction systems are undergoing sufficient trench migration to induce a three-dimensional return flow field beneath the slab, although trench migration rates are often imperfectly known and are highly dependent on the choice of reference frame [e.g., *Schellart et al.*, 2008; *Funiciello et al.*, 2008; *Long and Silver*, 2009]. This is a highly simplified view of sub-slab mantle dynamics and should only be thought of as providing a rough, first-order evaluation of the predictions of the 3-D return flow model.

Recent numerical modeling work has sought to understand the conditions under which three-dimensional return flow can create trench-parallel fast splitting directions beneath subducting slabs. *Paczkowski et al.* [2014] found that the geometry of sub-slab anisotropy varies as a function of the slab geometry (dip and depth extent), the background mantle flow, and the degree of mechanical coupling between the slab and the sub-slab mantle. A detailed comparison between the predictions of these numerical models and the splitting compilation presented in this study is underway. Nevertheless, our simplified framework, which approximates the sub-slab fast direction as roughly parallel to the local strike of the trench, provides a generally good first-order approximation for many subduction systems [*Paczkowski et al.*, 2014].

Another caveat to our modeling approach is that our model predictions are dependent on the subduction parameters used for each region (e.g., slab dip, lithospheric age, and convergence direction), and these

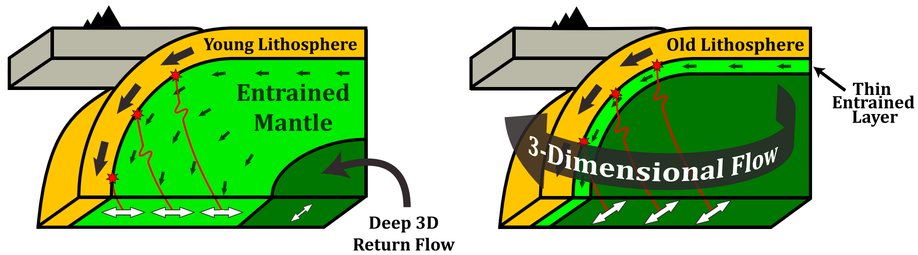

Figure 10. Schematic diagram of our preferred age-dependent flow model. (left) Beneath young (<95 Ma) lithosphere, downgoing slabs entrain a thick layer of mantle beneath them (light green). A deeper layer (dark green) participates in three-dimensional return flow induced by trench migration; however, direct S rays taking off from slab earthquakes mainly sample the entrained sub-slab layer, and the deeper layer does not contribute significantly to the observed anisotropy. This model would therefore predict fast directions that are mainly parallel to the motion of the downgoing plate (white arrows at bottom of diagram). (right) Beneath old (>95 Ma) lithosphere, the entrained layer is thin and the sub-slab mantle is efficiently decoupled from the downgoing slab. This allows for three-dimensional return flow (dark green layer) to dominate, and source-side splitting measurements (white arrows at bottom of diagram) mainly reflect dominantly trench-parallel flow directly beneath the slab.

parameters may be imperfectly known in some regions. In particular, the model variable that affects the predictions of the age-dependent and the strong radial anisotropy models most strongly is the direction of motion of the subducting plate. Defining this motion involves a choice of reference frame, and there is a great deal of debate over the most appropriate reference frame in which to assess plate motions (and other kinematic parameters that describe subduction). We have chosen to evaluate plate motions in the reference frame of the lower plate relative to the upper plate, as this is a natural choice for a subduction system. A different choice of reference frame, however, may impact the predictions of fast splitting direction for the strong radial anisotropy and age-dependent models. Further work on the choice of reference frame for kinematic variables in subduction systems may improve our understanding of this issue (see *Long and Silver* [2009] for a more detailed discussion of reference frames for subduction systems). While several simplifying assumptions are necessary in order to make predictions of splitting following the model setups described above, our results do capture the first-order characteristics of the various models and yield valuable insights into the dynamics of the sub-slab mantle.

Overall, our comparison between model predictions and splitting observations demonstrate that there is a correlation between sub-slab splitting behavior and subducting plate age and that an age-dependent model provides a better match to the observations than either the 3-D return flow model or the strong radial anisotropy model. Based on this observation, we propose a new conceptual model for sub-slab mantle dynamics that can explain the transition in splitting directions with plate age (Figure 10). We propose that beneath young (<95 Ma) subducting slabs, those slabs entrain a layer of sub-slab mantle as they subduct; this layer has a thickness on the order of ~200 km and is dominated by typical upper mantle olivine LPO fabrics (A-, C-, or E-type LPO) [e.g., *Karato et al*., 2008]. (In this study we have approximated these fabrics using an elastic tensor with hexagonal symmetry; a full investigation of the effect of different fabric types will be carried out in the future.) In this layer, simple shear deformation results in finite strain ellipses oriented parallel to the motion of the overriding plate, resulting in generally plate motion-parallel fast axes of anisotropy. Beneath this entrained layer, there may be a layer whose dynamics are controlled by trench migration; if the slab is rolling back, this layer will be dominated by three-dimensional return flow with a strong trench-parallel flow component. In turn, such a flow regime results in anisotropic fast axes that are generally aligned parallel to the trench. Several geodynamical modeling studies have provided evidence for such a complex flow regime [e.g., *Becker and Faccenna*, 2009; *Honda*, 2009; *Faccenda and Capitanio*, 2012, 2013; *Schellart and Moresi*, 2013; *Di Leo et al*., 2014; *Li et al*., 2014].

In such a multilayered system, the thickness of the respective layers and the raypaths used will determine the dominant splitting patterns. Beneath young oceanic lithosphere, we expect that direct S phases experiencing source-side shear wave splitting (i.e., the raypaths used in this study) will mainly sample the entrained layer directly beneath the slab, leading to plate motion-parallel fast directions (Figure 10, left). It is possible that other raypath geometries (e.g., SK(K)S phases for stations located on the overriding plate) may sample the deeper layer and reflect an integrated signal from both anisotropic regions. This may explain why different raypaths and phase types (i.e., SKS versus direct S) seem to reflect different splitting patterns for the same subduction system (e.g., Central America, as discussed in *Lynner and Long* [2014]).

Beneath older slabs (slabs with a lithospheric age of 95 Ma or older at a depth of 100 km), we hypothesize a change in the amount of mechanical coupling between the downgoing slab and the mantle beneath it. Specifically, we propose that old slabs are poorly coupled to (but not completely decoupled from) to the subjacent mantle; this decoupling may take the form of a thin, weak layer directly beneath the slab that accommodates the shear between the slab and the mantle beneath (Figure 10, right). If this layer is sufficiently thin, it will not contribute significantly to the observed anisotropy [e.g., *Long and Silver*, 2008, 2009]. For this case, we would expect much of the sub-slab mantle to be dominated by 3-D return flow if the trench is migrating with respect to the mantle around it. For the old lithosphere case, source-side S splitting measurements will mainly reflect anisotropy in the sub-slab layer dominated by 3-D return flow, and fast directions will be generally parallel to the trench (with some local complications due to slab morphology, complex strain geometry, and other factors).

Our age-dependent model for sub-slab anisotropy has interesting implications for our understanding of sub-slab mantle dynamics, as it implies different flow regimes beneath subducting slabs of different ages. If old slabs are poorly coupled to the mantle beneath them and therefore entrain little mantle material when they subduct, this has implications for global patterns of mantle flow and for models of mass transfer between the upper and lower mantle reservoirs. The age-dependent change in the nature of mechanical coupling beneath slab suggested by our model is important for both global and regional geodynamical models of sub-slab dynamics [e.g., *Becker and Faccenna*, 2009; *Honda*, 2009; *Schellart and Moresi*, 2013; *Faccenda and Capitanio*, 2012, 2013].

While this conceptual model does a good job of predicting the observed splitting patterns (right panels on Figure 6), the mechanism which controls the transition from entrained flow directly beneath the slab to weak mechanical coupling and thus mantle flow with a significant along-strike component at a lithospheric age of ~95 Ma needs to be explained. In particular, we seek a mechanism capable of explaining the relatively rapid transition from plate motion-parallel to trench-parallel splitting that we observe. This lateral transition is particularly dramatic in Kurile and in Sumatra [*Lynner and Long*, 2014] (see Figures 4 and 7), occurring over a length scale of a few hundred kilometers at most (and thus over a lithospheric age range of ~10 Ma). Importantly, this transition does not seem to be associated with either a decrease in delay time or a gradual rotation from plate motion-parallel to trench-parallel ϕ.

One potential mechanism that may be consistent with a relatively rapid transition in sub-slab dynamics at a lithospheric age of ~95 Ma is small-scale convection (SCC) beneath old oceanic lithosphere [e.g., *Korenaga and Jordan*, 2003; *van Hunen et al*., 2005; *van Hunen and Čadek*, 2009; *Wirth and Korenaga*, 2012]. SCC is a result of the increasing gravitational instability of old, cold, and dense oceanic lithosphere and results in small-scale upwellings and downwellings that dominate the flow field directly beneath the lithosphere. In this way, SCC can interfere with (and at least partially destroy) the usual mantle flow regime beneath oceanic lithosphere [e.g., *Huang et al*., 2003; *van Hunen et al*., 2005], which consists of simple shear between the moving plate and the mantle beneath it. Put another way, SSC can be thought of as acting to decrease the coupling of the motion of lithospheric plates from the mantle beneath it.

How might the onset of SSC affect the dynamics of the sub-slab mantle once a plate has begun to subduct? One possibility is that any amount of decoupling of the slab and subjacent mantle once subduction of a lithospheric plate begins is greatly enhanced by SSC. We envision a scenario in which the dynamics of the mantle beneath typical oceanic lithosphere is dominated by plate motion, even after the onset of SCC. Once the plate begins to subduct, however, the dynamics of the sub-slab mantle become much more complicated, and SCC may help to enhance decoupling in this complicated geometry. In this proposed scenario, subducting slabs may entrain less mantle (or entrain it less efficiently). Another related hypothesis is that if SSC results in warmer, less viscous asthenosphere directly beneath the lithosphere, when the slab begins to subduct it may entrain a thin layer of relatively low viscosity material, which acts as a decoupling layer (see discussions in *Long and Silver* [2009] and *Phipps Morgan et al*. [2013]). In any case, we suggest that beneath old lithosphere that has been affected by SSC, the slab is largely decoupled (although likely not entirely) from the mantle beneath it, allowing 3-D return flow to dominate. The idea that the coupling between oceanic lithosphere and the subjacent asthenospheric mantle (and thus the pattern of seismic anisotropy resulting from mantle flow) is disrupted beneath old lithosphere by SSC is supported by previous work. For example, *van Hunen and Čadek* [2009], motivated by the observation that azimuthal anisotropy beneath older lithosphere (40–60 Ma) in the Pacific is smaller than that beneath younger lithosphere [e.g., *Montagner*, 2002], showed that SSC can account for a reduction of azimuthal anisotropy beneath older lithosphere by a factor of 2 due to the disruption of the coherency of flow beneath lithosphere being acted upon by SSC. The dynamic effects of SSC are, however, still debated and more work is needed to understand the interplay of SSC, anisotropy, and mantle dynamics. The details of the dynamic regime beneath old slabs that have been affected by SSC remain to be explored, but it is plausible that the disruption of the usual lithosphere-asthenosphere coupling regime allows for a flow field similar to that shown in Figure 10 beneath old lithosphere.

The onset time of small-scale convection is still poorly constrained and subject to debate, although it has been studied both experimentally [e.g., *Davaille and Jaupart*, 1994] and numerically [e.g., *Korenaga and Jordan*, 2003]. Many complications exist in determining scaling laws for onset of SSC, such as the inclusion of temperature-dependent viscosity and the effects of shearing due to the motion of the overriding plate [e.g., *van Hunen et al.*, 2003]. The lack of consensus on the onset time of SSC makes it somewhat difficult to evaluate its plausibility as a mechanism for a change in sub-slab anisotropy, but a range of onset times from 50 Ma to 100 Ma have been suggested in the literature [e.g., *Ritzwoller et al.*, 2004; *Korenaga and Jordan*, 2004; *Dumoulin et al.*, 2005; *Korenaga*, 2009]. The onset time depends strongly on asthenospheric viscosity and activation energy, leading to large uncertainties, as both parameters are poorly known [*Dumoulin et al.*, 2005; *Korenaga*, 2009]. It is also worth noting that after the onset of SSC, the longitudinal rolls of SSC grow in size with increasing time [*Korenaga and Jordan*, 2003]. It may be that SSC needs to be acting for some amount of time in order for convection to be sufficiently vigorous and acting on a large enough volume of mantle to sufficiently disrupt the coherency of flow directly beneath the plate to decrease the coupling between the slab and the subjacent mantle. In any case, given the range of onset times that have been suggested and the age at which we observe a transition in sub-slab splitting behavior (~95 Ma), SSC may be a plausible mechanism to explain the difference in behavior.

An age-controlled transition in sub-slab splitting behavior has been previously suggested based on the observation of predominantly plate motion-parallel fast SKS splitting directions beneath Cascadia and Mexico. Specifically, *Long and Silver* [2009] proposed a transition to predominantly trench-parallel fast splitting directions at a lithospheric age of ~10 Ma. Most of the sub-slab splitting estimates used in the *Long and Silver* [2009] compilation were based on SK(K)S measurements that had been corrected for the effect of wedge anisotropy. Based on our more recent and more accurate source-side splitting compilation, we suggest here instead a transition in sub-slab splitting behavior at a considerably larger lithospheric age of ~95 Ma.

In this paper we have discussed the possibility that the onset of small-scale convection may provide a mechanism for partially decoupling older slabs from the mantle beneath them and suppressing the entrainment of sub-slab mantle. Other mechanisms may be possible, however, and the nature and extent of mechanical coupling between the oceanic lithosphere and the asthenospheric mantle beneath it remains poorly understood. The question of how well plates are coupled to the asthenosphere beneath them is intimately related to questions surrounding the nature of the lithosphere, asthenosphere, and the boundary between them, which remain poorly understood [e.g., *Fischer et al.*, 2010]. Various models for the nature of the asthenosphere have been proposed based on seismologic observations of the oceanic lithosphere-asthenosphere boundary (LAB), which generally yield evidence for a sharp boundary with a large velocity contrast [e.g., *Kawakatsu et al.*, 2009; *Rychert and Shearer*, 2009, 2011; *Schmerr*, 2012]. Various models have been proposed to explain the nature of the LAB, including those that invoke the presence of partial melt in the asthenosphere [e.g., *Kawakatsu et al.*, 2009; *Schmerr*, 2012; *Naif et al.*, 2013] or a role for grain boundary sliding [*Karato*, 2012; *Olugboji et al.*, 2013]. The dynamic behavior of the sub-slab mantle, as manifested in seismic anisotropy, is likely controlled at least in part by the nature of the oceanic asthenosphere and the LAB, and further work on the nature of the oceanic lithosphere-asthenosphere system is crucial to our understanding of sub-slab mantle flow.

6. Summary

Understanding the dynamics of the sub-slab mantle is of utmost importance to our understanding of subduction systems and how subducting slabs interact with the surrounding mantle. In this study, we have compiled a data set composed of detailed measurements of seismic anisotropy beneath subducting slabs from previously published source-side shear wave splitting studies [*Foley and Long*, 2011; *Lynner and Long*, 2013, 2014]. We used this compilation to test the predictions of three plausible models for sub-slab anisotropy and mantle dynamics: the strong radial anisotropy model of *Song and Kawakatsu* [2012], which invokes two-dimensional entrained mantle flow beneath slabs, the 3-D return flow model [*Russo and Silver*, 1994; *Long and Silver*, 2008, 2009], which argues for generally trench-parallel strain beneath slabs, and a new age-dependent anisotropic model, which invokes a difference in sub-slab mantle flow patterns beneath slabs of different lithospheric ages.

We generated predictions of fast splitting directions for 623 direct S rays in our compilation that exhibited source-side sub-slab shear wave splitting and compared them to the observations; our model comparisons included the Tonga, Caribbean, Scotia, Alaska-Aleutians, Central America, Kurile, Northern Honshu, Izu-Bonin, Ryukyu, and Sumatra subduction zones. We found that the age-dependent model provides the best fit to the observations globally; when individual subduction zones are considered, the age-dependent model was found to be the best fitting model for all regions except Scotia and the Caribbean. For the global data set, the age-dependent model successfully matched 34.2% of the model predictions, with an average misfit of 27.7°. The other two models were less successful at matching the observations, with the strong radial anisotropy model matching 23.8% of the measurements with an average misfit of 37.6° and the 3-D return flow model matching 14.8% of the observations with an average misfit of 45.7°.

Based on this observation, we propose two distinctive regimes of anisotropy and mantle flow beneath subducting slabs. Beneath young slabs ($>$95 Ma), we suggest that slabs entrain a thick layer of sub-slab mantle. In this layer, the finite strain orientations align locally with the plate motion and slab dip, while A-, C-, or E-type olivine fabrics dominate in the sub-slab mantle. Beneath this entrained layer, we propose that there is deeper region of sub-slab that participates in three-dimensional return flow induced by trench migration. For younger slabs, source-side shear wave splitting measurements mainly sample the entrained layer, resulting in fast directions that are generally parallel to the motion of the downgoing slab. Beneath older slabs ($>$95 Ma), we propose that the sub-slab mantle is sufficiently decoupled from the slab itself to enable three-dimensional return mantle flow directly beneath the slab. Source-side measurements for these systems mainly sample sub-slab flow with a strong trench-parallel component, resulting in dominantly trench-parallel fast splitting directions. This sub-slab decoupling beneath old lithosphere is likely accommodated via a substantial thinning of the sub-slab entrained layer, such that it does not contribute significantly to the observed splitting.

A possible mechanism for the difference in mechanical coupling beneath old versus young slabs is the onset of small-scale convection beneath old oceanic lithosphere, but the details remain unclear, and other mechanisms may be possible. We suggest that the dynamic behavior of the mantle beneath subducting slabs is likely intimately related to the properties of the oceanic LAB and the oceanic asthenosphere, which remain to be fully understood. Future work on the dynamics of the sub-slab mantle that includes more realistic slab morphologies and flow fields and investigates different olivine fabric types should continue to shed light on this important aspect of subduction systems.

Acknowledgments

Many figures in the study were prepared using the Generic Mapping Tools [*Wessel and Smith*, 1999]. This work was funded by NSF grant EAR-1150722. We thank Shun Karato, David Bercovici, David Evans, and Jeffrey Park for useful discussions on sub-slab anisotropy and dynamics. We are grateful to Manuele Faccenda, an anonymous reviewer, and the Associate Editor for helpful comments that improved the manuscript.

References

Abt, D. L., K. M. Fischer, G. A. Abers, M. Protti, V. González, and W. Strauch (2010), Constraints on upper mantle anisotropy surrounding the Cocos slab from SK(K)S splitting, *J. Geophys. Res.*, *115*, B06316, doi:10.1029/2009JB006710.

Becker, T. W., and C. Faccenna (2009), A review of the role of subduction dynamics for regional and global plate motions, in *Subduction Zone Geodynamics*, edited by S. Lallemand and F. Funiciello, pp. 3–34, Springer, Berlin Heidelberg, Germany.

Buttles, J., and P. Olson (1998), A laboratory model of subduction zone anisotropy, *Earth Planet. Sci. Lett.*, *164*, 245–262.

Chevrot, S., and R. D. Van Der Hilst (2003), On the effects of a dipping axis of symmetry on shear wave splitting measurements in a transversely isotropic medium, *Geophys. J. Int.*, *152*, 497–505.

Crotwell, H. P., T. J. Owens, and J. Ritsema (1999), The TauP toolkit: Flexible seismic travel-time and ray-path utilities, *Seismol. Res. Lett.*, *70*, 154–160.

Cruciani, C., E. Carminati, and C. Doglioni (2005), Slab dip vs lithosphere age: No direct function, *Earth Planet. Sci. Lett.*, *238*, 298–310.

Davaille, A., and C. Jaupart (1994), Onset of thermal convection in fluids with temperature- dependent viscosity: Application to the oceanic mantle, *J. Geophys. Res.*, *99*, 19,853–19,866, doi:10.1029/94JB01405.

DeMets, C., R. G. Gordon, and D. F. Argus (2010), Geologically current plate motions, *Geophys. J. Int.*, *181*, 1–80, doi:10.1111/j.1365-246X.2009.04491.x.

Di Leo, J. F., J. Wookey, J. O. S. Hammond, J.-M. Kendall, S. Kaneshima, H. Inoue, T. Yamashina, and P. Harjadi (2012), Deformation and mantle flow beneath the Sangihe subduction zone from seismic anisotropy, *Phys. Earth Planet. Int.*, *194–195*, 38–54.

Di Leo, J. F., A. M. Walker, Z.-H. Li, J. Wookey, N. M. Ribe, J.-M. Kendall, and A. Tommasi (2014), Development of texture and seismic anisotropy during the onset of subduction, *Geochem. Geophys. Geosyst.*, *15*, 192–212, doi:10.1002/2013GC005032.

Dumoulin, C., M. P. Doin, D. Arcay, and L. Fleitout (2005), Onset of small-scale instabilities at the base of the lithosphere: Scaling laws and role of pre-existing lithospheric structures, *Geophys. J. Int.*, *160*, 345–357, doi:10.1111/j.1365-246X.2004.02475.x.

Eakin, C. M., and M. D. Long (2013), Complex anisotropy beneath the Peruvian flat slab from frequency-dependent, multiple-phase shear wave splitting analysis, *J. Geophys. Res. Solid Earth*, *118*, 4794–4813, doi:10.1002/jgrb50349.

Faccenda, M., and F. A. Capitanio (2012), Development of mantle seismic anisotropy during subduction-induced 3-D flow, *Geophys. Res. Lett.*, *39*, L11305, doi:10.1029/2012GL051988.

Faccenda, M., and F. A. Capitanio (2013), Seismic anisotropy around subduction zones: Insights from three-dimensional modeling of upper mantle deformation and SKS splitting calculations, *Geochem. Geophys. Geosyst.*, *14*, 243–262, doi:10.1029/2012GC004451.

Faccenda, M., L. Burlini, T. V. Gerya, and D. Mainprice (2008), Fault-induced seismic anisotropy by hydration in subducting oceanic plates, *Nature*, *455*, 1097–1100.

Fischer, K. M., H. A. Ford, D. L. Abt, and C. A. Rychert (2010), The lithosphere-asthenosphere boundary, *Annu. Rev. Earth Planet. Sci.*, *38*, 551–575.

Foley, B. J., and M. D. Long (2011), Upper and mid-mantle anisotropy beneath the Tonga slab, *Geophys. Res. Lett.*, *38*, L02303, doi:10.1029/2010GL046021.

Funiciello, F., C. Faccenna, A. Heuret, S. Lallemand, E. Di Giuseppe, and T. W. Becker (2008), Trench migration, net rotation and slab–mantle coupling, *Earth Planet. Sci. Lett.*, *271*, 233–240.

Gudmundsson, O., and M. Sambridge (1998), A regionalized upper mantle (RUM) seismic model, *J. Geophys. Res.*, *103*, 7121–7136, doi:10.1029/97JB02488.

Healy, D., S. M. Reddy, N. E. Timms, E. M. Gray, and A. Vitale Brovarone (2009), Trench-parallel fast axes of seismic anisotropy due to fluid-filled cracks in subducting slabs, *Earth Planet. Sci. Lett.*, *283*, 75–86.

Heuret, A., and S. Lallemand (2005), Plate motions, slab dynamics and back-arc deformation, *Phys. Earth Planet. Int.*, *149*, 31–51, doi:10.1016/j.pepi.2004.08.022.

Honda, S. (2009), Numerical simulations of mantle flow around slab edges, *Earth Planet. Sci. Lett.*, *277*(1–2), 112–122, doi:10.1016/j.epsl.2008.10.003.

Huang, J., S. Zhong, and J. van Hunen (2003), Controls on sub-lithospheric small-scale convection, *J. Geophys. Res.*, *108*(B8), 2405, doi:10.1029/2003JB002456.

Jung, H., W. Mo, and H. W. Green (2009), Upper mantle seismic anisotropy resulting from pressure-induced slip transition in olivine, *Nat. Geosci.*, *2*, 73–77.

Karato, S. (2012), On the origin of the asthenosphere, *Earth Planet. Sci. Lett.*, *321–322*, 95–103.

Karato, S., H. Jung, I. Katayama, and P. Skemer (2008), Geodynamic significance of seismic anisotropy of the upper mantle: New insights from laboratory studies, *Annu. Rev. Earth Planet. Sci.*, *36*, 59–95.

Kawakatsu, H., P. Kumar, Y. Takei, M. Shinohara, T. Kanazawa, E. Araki, and K. Suyehiro (2009), Seismic evidence for sharp lithosphere-asthenosphere boundaries of oceanic plates, *Science*, *324*, 499–502.

Kennett, B. L. N., and E. R. Engdahl (1991), Traveltimes for global earthquake location and phase identification, *Geophys. J. Int.*, *105*, 429–465.

Korenaga, J. (2009), How does small-scale convection manifest in surface heat flux?, *Earth Planet. Sci. Lett.*, *287*(3–4), doi:10.1016/j.epsl.2009.08.015.

Korenaga, J., and T. H. Jordan (2003), Physics of multiscale convection in Earth's mantle: Onset of sublithospheric convection, *J. Geophys. Res.*, *108*(B7), 2333, doi:10.1029/2002JB001760.

Korenaga, J., and T. H. Jordan (2004), Physics of multiscale convection in Earth's mantle: Evolution of sublithospheric convection, *J. Geophys. Res.*, *109*, B01405, doi:10.1029/2003JB002464.

Lallemand, S., A. Heuret, and D. Boutelier (2005), On the relationships between slab dip, back-arc stress, upper plate absolute motion, and crustal nature in subduction zones, *Geochem. Geophys. Geosyst.*, *6*, Q09006, doi:10.1029/2005GC000917.

Li, Z.-H., J. F. Di Leo, and N. M. Ribe (2014), Subduction-induced mantle flow, finite strain, and seismic anisotropy: Numerical modeling, *J. Geophys. Res. Solid Earth*, *119*, 5052–5076, doi:10.1002/2014JB010996.

Long, M. D. (2013), Constraints on subduction geodynamics from seismic anisotropy, *Rev. Geophys.*, *51*, 76–112, doi:10.1002/rog.20008.

Long, M. D., and P. G. Silver (2008), The subduction zone flow field from seismic anisotropy: A global view, *Science*, *319*, 315–318.

Long, M. D., and P. G. Silver (2009), Mantle flow in subduction systems: The sub-slab flow field and implications for mantle dynamics, *J. Geophys. Res.*, *114*, B10312, doi:10.1029/2008JB006200.

Long, M. D., and E. A. Wirth (2013), Mantle flow in subduction systems: The wedge flow field and implications for wedge processes, *J. Geophys. Res. Solid Earth*, *118*, 583–606, doi:10.1002/jgrb.50063.

Lynner, C., and M. D. Long (2013), Sub-slab seismic anisotropy and mantle flow beneath the Caribbean and Scotia subduction zones: Effects of slab morphology and kinematics, *Earth Planet. Sci. Lett.*, *361*, 367–378, doi:10.1016/j.epsl.2012.11.007.

Lynner, C., and M. D. Long (2014), Sub-slab anisotropy beneath the Sumatra and circum-Pacific subduction zones from source-side shear wave splitting observations, *Geochem. Geophys. Geosyst.*, *15*, 2262–2281, doi:10.1002/2014GC005239.

McCormack, K., E. A. Wirth, and M. D. Long (2013), B-type olivine fabric and mantle wedge serpentinization beneath the Ryukyu arc, *Geophys. Res. Lett.*, *40*, 1697–1702, doi:10.1002/grl.50369.

Miller, M. S., and T. W. Becker (2012), Mantle flow deflected by interactions between subducted slabs and cratonic keels, *Nat. Geosci.*, *19*, 726–730, doi:10.1038/nego01553.

Montagner, J. P. (2002), Upper mantle low anisotropy channels below the Pacific Plate, *Earth Planet. Sci. Lett.*, *202*(2), 263–274.

Müller, C., B. Bayer, A. Eckstaller, and H. Miller (2008a), Mantle flow in the South Sandwich subduction environment from source-side shear wave splitting, *Geophys. Res. Lett. 35*, L03301, doi:10.1029/2007GL032411.

Müller, R. D., M. Sdrolias, C. Gaina, and W. R. Roest (2008b), Age spreading rates and spreading asymmetry of the world's ocean crust, *Geochem. Geophys. Geosys.*, *9*, Q04006, doi:10.1029/2007GC001743.

Naif, S., K. Key, S. Constable, and R. L. Evans (2013), Melt-rich channel observed at the lithosphere-asthenosphere boundary, *Nature*, *495*, 356–359.

Olugboji, T. M., S. Karato, and J. Park (2013), Structures of the oceanic lithosphere-asthenosphere boundary: Mineral-physics modeling and seismological signatures, *Geochem. Geophys. Geosyst.*, *14*, 880–901, doi:10.1002/ggge.20086.

Paczkowski, K., L. G. J. Montesi, M. D. Long and C. J. Thissen (2014), Three-dimensional flow in the sub-slab mantle, *Geochem. Geophys. Geosyst*., doi:10.1002/2014GC005441.

Peyton, V., V. Levin, J. Park, M. Brandon, J. Lees, E. Gordeev, and A. Ozerov (2001), Mantle flow at a slab edge: Seismic anisotropy in the Kamchatka region, *Geophys. Res. Lett.*, *28*, 379–382, doi:10.1029/2000GL012200.

Phipps Morgan, J., H. Hasenclever, and C. Shi (2013), New observational and experimental evidence for a plume-fed asthenosphere boundary layer in mantle convection, *Earth Planet. Sci. Lett.*, *366*, 99–111.

Ritzwoller, M. H., N. M. Shapiro, and S.-J. Zhong (2004), Cooling history of the Pacific lithosphere, *Earth Planet. Sci. Lett.*, *226*, 69–84.
Russo, R. M. (2009), Subducted oceanic asthenosphere and upper mantle flow beneath the Juan de Fuca slab, *Lithosphere*, *1*, 195–205.
Russo, R. M., and P. G. Silver (1994), Trench-parallel flow beneath the Nazca plate from seismic anisotropy, *Science*, *263*, 1105–1111.
Russo, R. M., A. Gallego, D. Comte, V. I. Moncau, R. E. Murdie, and J. C. VanDecar (2010), Source-side shear wave splitting and upper mantle flow in the Chile Ridge subduction zone, *Geology*, *38*, 707–710.
Rychert, C. A., and P. M. Shearer (2009), A global view of the lithosphere-asthenosphere boundary, *Science*, *324*, 495–498.
Rychert, C. A., and P. M. Shearer (2011), Imaging the lithosphere-asthenosphere boundary beneath the Pacific using SS waveform modeling, *J. Geophys. Res.*, *116*, B07307, doi:10.1029/2010JB008070.
Schellart, W. P., and L. Moresi (2013), A new driving mechanism for backarc extension and backarc shortening through slab sinking induced toroidal and poloidal mantle flow: Results from dynamic subduction models with an overriding plate, *J. Geophys. Res. Solid Earth*, *118*, 3221–3248, doi:10.1002/jgrb.50173.
Schellart, W. P., D. R. Stegman, and J. Freeman (2008), Global trench migration velocities and slab migration induced upper mantle volume fluxes: Constraints to find an Earth reference frame based on minimizing viscous dissipation, *Earth Sci. Rev.*, *88*, 118–144.
Schmerr, N. (2012), The Gutenberg discontinuity: Melt at the lithosphere-asthenosphere boundary, *Science*, *335*, 1480–1483.
Silver, P. G., and W. W. Chan (1991), Shear wave splitting and subcontinental mantle deformation, *J. Geophys. Res.*, *96*, 16,429–16,454, doi:10.1029/91JB00899.
Song, T.-R. A., and H. Kawakatsu (2012), Subduction of oceanic asthenosphere: Evidence from sub-slab seismic anisotropy, *Geophys. Res. Lett.*, *39*, L17301, doi:10.1029/2012GL052639.
Song, T.-R. A., and H. Kawakatsu (2013), Subduction of oceanic asthenosphere: A critical appraisal in central Alaska, *Earth Planet. Sci. Lett.*, *367*, 82–94.
Ulmer, P., and V. Trommsdorff (1995), Serpentine stability to mantle depths and subduction-related magmatism, *Science*, *268*, 858–61.
van Hunen, J., and O. Čadek (2009), Reduced oceanic seismic anisotropy by small-scale convection, *Earth Planet. Sci. Lett.*, *284*, 622–629, doi:10.1016/j.epsl.2009.05.034.
van Hunen, J., J. S. Huang, and S. J. Zhong (2003), The effect of shearing on the onset and vigor of small-scale convection in a Newtonian rheology, *Geophys. Res. Lett.*, *30*(19), 1991, doi:10.1029/2003GL018101.
van Hunen, J., S. Zhong, N. M. Shapiro, and M. H. Ritzwoller (2005), New evidence for dislocation creep from 3-D geodynamic modeling of the Pacific upper mantle structure, *Earth Planet. Sci. Lett.*, *238*, 146–155.
Vinnik, L. P., and R. Kind (1993), Ellipticity of teleseismic S-particle motion, *Geophys. J. Int.*, *113*, 165–174.
Vinnik, L., R. Kind, G. L. Kosarev, and L. Makeyeva (1989), Azimuthal anisotropy in the lithosphere from observations of long-period S-waves, *Geophys. J. Int.*, *99*, 549–559.
Walker, A., and J. Wookey (2012), MSAT-A new toolkit for the analysis of elastic and seismic anisotropy, *C. R. Geosci.*, *49*, 81–90.
Wessel, P., and W. H. F. Smith (1999), Free software helps map and display data, *Eos Trans. AGU*, *72*, 441, doi:10.1029/90EO00319.
Wirth, E. A., and J. Korenaga (2012), Small-scale convection in the subduction zone mantle wedge, *Earth Planet. Sci. Lett.*, *357–358*, 111–118.
Wirth, E. A., and M. D. Long (2012), Multiple layers of seismic anisotropy and a low-velocity region in the mantle wedge beneath Japan: Evidence from teleseismic receiver functions, *Geochem. Geophys. Geosyst.*, *13*, Q08005, doi:10.1029/2012GC004180.

